An EBSD analysis of a commercial immiscible Cu43%Cr alloy after high-pressure torsion processing and annealing

I. Bibimoune[1*], K. Abib[1], T. Baudin[2], F. Brisset[2], Y. Huang[3,4], D. Bradai[1], T. G. Langdon[4]

[1] Laboratory of Materials Physics, Faculty of Physics, University of Sciences and Technology Houari Boumediene, BP 32, El Alia, Bab Ezzouar, 16111 Algiers, Algeria.

[2] Université Paris-Saclay, CNRS, Institut de chimie moléculaire et des matériaux d'Orsay, 91405 Orsay, France

[3] Department of Design and Engineering, Faculty of Science and Technology, Bournemouth University, Poole, Dorset BH12 5BB, UK

[4] Materials Research Group, Department of Mechanical Engineering, University of Southampton, Southampton SO17 1BJ, UK

[*]Corresponding author : imenebibimoune2017@gmail.com

Abstract

The influence of high-pressure torsion (HPT) and annealing on microstructure, texture and thermal stability of an immiscible composite Cu43%Cr alloy was studied using electron backscatter diffraction, X-ray diffraction and microhardness measurements. As-received alloy samples were subjected to HPT and subsequent annealing treatment in the range of 210 to 850 °C for 1 hour in order to develop ultrafine-grained (UFG) microstructures and highlight their thermal stability. The Cu and Cr grains were refined to ~0.45 and ~0.39 µm, respectively and exhibited equiaxed morphology. The crystallographic texture was of shear type in both Cu and Cr with the domination of C and F orientations, respectively. The UFG microstructure and texture were retained in the Cu43%Cr alloy up to 850 °C. The global results show that the immiscible composite Cu43%Cr alloy exhibits a high thermal stability up to 850°C. The evolution of the microstructure, texture and thermal stability of the UFG Cu43%Cr alloy was compared to published data and available models.

Keywords: CuCr alloy, high-pressure torsion, annealing, microstructure, texture, thermal stability.

1. Introduction

The CuCr immiscible alloys have attracted much interest for their excellent mechanical strength combined with the high electrical and thermal conductivity, which are essential for highly mechanically-stressed electrical devices. Thus, these alloys are mainly used in contact cables [1], as lead frames in integrated circuits [2] and as electric contacts in high voltage electrical circuits [3, 4].

Severe plastic deformation (SPD) techniques have been recognized as the best procedures for producing exceptional grain refinement to the nanometer level in many metals and alloys. In practice, it is well established that the grain refinement through SPD processing to the nanometer scale improves the mechanical (strength, hardness) properties while the physical properties (electrical conductivity) are only mildly affected [5].

These SPD techniques have been used to fabricate immiscible nanostructured materials such as Cu-Nb [6], Cu-Fe [7], Cu-Ta [8], Zr-Nb [9] and Cu-Cr [10]. The most widely used techniques are equal-channel angular pressing (ECAP) [11], accumulative roll bonding (ARB) [12] and high-pressure torsion (HPT) [13, 14]. The latter procedure is one of the most effective mechanical alloying techniques for inducing substantial level of strain and strong grain refinement down to the sub-micrometer and/or the nanometer scale. In the HPT technique, samples in the form of disks are subjected simultaneously to a high hydrostatic pressure of a few GPa and a torsional shear stress. Moreover, the HPT technique may cause the forced intermixing for immiscible alloys [15, 16] and therefore the deformation mechanisms of UFG and/or nanostructured crystalline (NC) metals and alloys may differ from coarse grained (CG). The operating mechanisms in UFG and NC materials are up to now controversial [17].

Many studies have used a complete panel of characterization methods, including atom probe tomography (APT), X-ray diffraction (XRD), energy-dispersive synchrotron diffraction (EDXS), high resolution and scanning electron microscopy transmission (HRTEM, STEM) to exhaustively investigate the phase fraction changes, nanostructures and sub-micrometer scale compositions [10, 17, 18, 19] in immiscible Cu43%Cr alloy. For example, it was shown that, when samples were deformed up to 25 rotations, the average grain size was decreased dramatically from the micron-scale at a few tens of microns to around 20 nm [10] and there was only a slight further refinement to an average size of around 10 nm when the sample was severely deformed up to 100 rotations. These grain sizes are one order of magnitude smaller than in commercially pure metals processed by HPT [5] indicating that the interphase boundaries play a critical role in the grain size reduction mechanism [18].

It was further stated that grain refinement in Cu was governed by the interaction between Cr solutes (or clusters) that were forced to dissolve into the Cu matrix and prolonged dislocations motion during the early deformation stage [17]. However, at these higher strain conditions, complicated mechanisms involving solute effects and constraint effects during SPD processing were responsible for the grain refinement of Cu and Cr.

It was also established [7, 10, 18, 19] that super-saturated solid solutions (SSSSs) of up to 15 at% (17.7 wt%) Cu in the body-centered cubic (bcc) Cr phase were formed but the formation of SSSSs of Cr in the face-centered cubic (FCC) Cu phase was very restricted (<5%). The formation of SSSS during HPT is mainly controlled by a mechanical mixing mechanism and the amount of mixing is controlled by the strain level [19].

In situ structural (STEM) and spectroscopic (EELS) investigations substantially demonstrated that the bulk NC materials evolve chemically and structurally with temperature as well as establishing the mechanism of thermal stability [20]. This study highlighted the correlations between the thermal stability and chemical decomposition process of bulk

nanostructured materials. The final grain size of nanostructured materials is governed by their thermal stability [21] and this is an important problem from the point of view of the practical applications of nanomaterials [21].

The thermal stability at the atomic resolution of Cu43%Cr processed by HPT was studied together with subsequent in situ annealing at 25, 210 and 414 °C using Electron-Energy-Loss Spectroscopy (EELS) [20]. It was reported that a chemical destabilization of supersaturated CuCr nanocrystals occurs at a fairly low temperature (210°C). Thus, the supersaturated CuCr nanocrystals lose their chemical stability soon after annealing at 210°C and there is a rapid separation of Cu and Cr grains at the forced intermixing zone, concomitant to a thinning of the interface width while no noticeable grain growth occurred.

The thermal stability of UFG and/or NC metals and alloys fabricated by SPD techniques is associated with the generated defects and stored energy [22, 23] and the stability aspects of bulk nanostructured materials have been widely reviewed [21, 24-26]. There is a report that the Cu43%Cr alloy processed by HPT up to 25 turns and aged for 30 min at 450 °C experienced some grain growth that occurred during ageing but with the grain size remaining in the range of 20–40 nm [18].

Based on this review, the aim of the present research was to study the microstructure and texture of an immiscible composite Cu43%Cr alloy after HPT processing up to 20 turns and annealing. Special attention was given to investigating, at a more extended scale than with atomic resolution, the thermal stability of the UFG Cu43%Cr alloy through electron backscatter diffraction, microhardness measurements and X-ray diffraction experiments.

2. Experimental material and procedures

A commercial Cu43%Cr (wt.%) alloy was provided by PLANSEE (Reutte, Austria) in the form of cylinders. Disks of 10 mm in diameter and 1 mm in thickness were machined from

the as-received material using an electrical discharge device and these samples were then subjected to HPT at room temperature up to 5 and 20 turns. After HPT deformation, annealing was carried out at various temperatures of 210, 550 and 850 °C under an inert argon atmosphere for 1 h. The principle of HPT processing is illustrated in Figure 1 which shows that a disk sample undergoes torsional shear deformation under a high hydrostatic pressure which was set at 6 GPa.

Electron back-scatter diffraction (EBSD) measurements were performed near the mid-radius of the disks on 100 × 60 (as-received), 100 × 100 (N=5) and 40 × 40 µm² (N=20 turns) zones perpendicular to the HPT rotation axis. A Scanning Electron Microscope (SEM) was used with a Field Emission Gun (FEG) SUPRA 55 VP operating at 20 kV with a TSL orientation imaging system using OIM™ software. The step size was 100 nm for the as received sample and for N=5 turns and 50 nm for N=20 turns. The quantitative texture analysis was carried out by calculating the Orientation Distribution Function (ODF). All datum points with a confidence index (CI) lower than 0.05 were excluded from the analysis where CI quantifies the reliability of the indexed patterns. A grain dilation and grain Confidence Index standardization clean- up with a grain tolerance of 5° and a minimum grain size of 5 pixels were applied to improve the quality of the EBSD raw data.

X-ray diffraction (XRD) experiments were conducted on the as received, HPT-processed and annealed samples on a PANalytical X'Pert3 Diffractometer (Eùpyrean) with Cu Kα1 radiation (0.154059 nm) operating at 30 mA and 40 kV. The X-ray step size and time were 0.013° and 1s, respectively in the 2θ angle range of 30 – 100°. The analyzed zone was close to the mid-radius and the irradiated length of the divergence slit was 0.5 mm. A refinement of the XRD patterns was performed using a Rietveld method implemented in the MAUD (Material Analysis Using Diffraction) software [27]. The instrumental broadening measured on some standard sample (silicon powder, SRMR 640c, Topsil Semiconductor Materials, A/S, Frederikssund,

Denmark) is usually simply parametrised and treated by analytical profile functions, which are convoluted with the microstructural effects.

This refinement allowed an assessment of the crystallite size, microstrain and the lattice parameter for the Cu and Cr phases.

The dislocation density was calculated from an equation which assumes the average dislocation density, ρ, of the microstructure is a function of microstrain and crystallite size [28]:

$$\rho = (\rho_D \, \rho_\varepsilon)^{1/2} \qquad (1)$$

where $\rho_D = 3/D^2$ and $\rho_\varepsilon = k\varepsilon^2/Fb^2$. Here, $k = 6\pi$, $F = 1$, b is the magnitude of the Burgers vector, D is the crystallite size and ε is the microstrain.

Vickers microhardness (Hv) measurements were taken with a load of 0.98 N maintained for 10 s using a Zwick 3212 microhardness tester. For HPT samples, measurements near the mid-radius of disks were taken, at every measurement and the average microhardness was determined from four separate measurements clustered uniformly around the selected position.

<Figure 1>

3. Experimental Results

3.1 Microstructure and texture of the Cu-Cr alloy in the as-received state

Figure 2 (a-c) presents the inverse pole figure (CD-IPF) maps of the Cu43%Cr before deformation. The initial microstructure shows a bimodal grain size distribution and the Cu phase significantly contains fine equiaxed grains while a large fraction of coarse grains are present in the Cr phase. From Figure 3 (a-b), the initial texture of the Cu phase shows a near {110}<112> Brass and {110}<001>Goss components with a maximum of 9.8 mrd (Multiple of a Random Distribution). The texture of the Cr phase exhibits a dominant {001}<010> orientation with a maximum of 6.7 mrd and a minor {111}<110> orientation which belongs to

the γ-fibre of BCC structure. These microstructures and texture are due to the specific manufacturing process that probably incorporates different thermo-mechanical steps. Figure 2c shows the histograms of the misorientation angles (Fv stems for volume fraction of misorientation angles) of the Cu and Cr phases in the as-received state. It is obvious that their distributions are not random given by the solid line and nearly 50% of the grain boundaries are of low-angle type which results from the generation of dislocations during the manufacturing.

<Figure 2>

<Figure 3>

3.2 Microstructure and texture of Cu-Cr alloy after HPT processing and annealing

Figs 4 and 5 present the inverse pole figure (CD-IPF) maps which depict the microstructures of the Cu and Cr phases of the Cu43%Cr alloy after N=5 and 20 turns of HPT processing and annealing up to 850°C, respectively. After HPT processing up to N=5 turns (Fig. 4 at 25°C), the EBSD analysis reveals the existence of wide zones with mainly Cu or Cr phases.

<Figure 4>

<Figure 5>

The evolutions of the mean grain size and the fraction of high-angle grain boundaries (HAGB) as a function of the number of HPT turns and annealing temperature are shown in Figure 6. After straining, the grains experienced a significant refinement soon after 5 HPT turns. In the as-received state, the grain size was 0.9 and 3.9 μm, for Cu and Cr phases, respectively. These values decrease to 0.6 and 1.1 μm and to 0.45 and 0.39 μm, after 5 and 20 HPT turns, respectively. After annealing, the grain size is apparently stable.

<Figure 6>

It is known that the relative amounts of high (HAGB) and low (LAGB) angle grain boundaries as a function of deformation strain can be used to clarify the processes involved in the microstructural evolution upon SPD processing and/or annealing [29]. Thus, the fraction of

HAGB in the Cu phase varied from 38% (N=0) to 71% and 62 % and in Cr phase from 33% (N=0) to 48% and 54% after 5 and 20 turns, respectively. The achieved HAGB values are very close to reported ones (~68%) for a Cu-2.5%Ni-0.6%Si alloy (wt.%) after HPT [30] up to 10 turns and (70%) for Cu-1Cr-0.1Zr (wt.%) [31] processed by ECAP (route Bc) and to the value reported (~ 60 %) for a Fe-36%Ni (wt. %) alloy processed by ARB [32].

<Figure 7>

Figure 7 shows the evolution of the grain boundary misorientation angles after HPT processing and annealing of the Cu43%Cr alloy after HPT processing up to N=5 and 20 turns and annealing. It is evident from these histograms that there remains a large fraction of low-angle boundaries in all disk samples even after processing through 5 and 20 turns but nevertheless there is no gradual evolution towards higher misorientation angles with annealing.

3.3 Texture evolution of the CuCr alloy after HPT processing and annealing

<Figure 8>

<Figure 9>

Figures 8 and 9 show the crystallographic texture evolution of the Cu43%Cr alloy after HPT processing up to N=5 and N=20 and annealing up to 850°C, respectively. The ODF section of the annealed alloy at 210°C is not presented since it resembles that of the as deformed state. An exhaustive review of the texture formation after HPT processing for several materials with FCC, BCC and HCP structures was published earlier [14]. The shear texture in FCC materials is typically formed of A, $\overline{\mathrm{A}}$, A_1^* , A_2^*, B, $\overline{\mathrm{B}}$ and C components [33, 34]. These are described in terms of the {hkl}〈uvw〉 representation where the {hkl} plane and 〈uvw〉 direction are parallel to the shear plane and shear direction, respectively. The above cited texture orientations belong to two fibres: an A-fibre ({111}// SP), where SP is the shear plane (or defined as the SD-RD plane) containing A, $\overline{\mathrm{A}}$, A_1^* and A_2^* components and a B-fibre (〈110〉//SD) with A, $\overline{\mathrm{A}}$, B, $\overline{\mathrm{B}}$ and C components.

The shear texture for BCC materials can be well described also by two fibres. The first fibre is {110}//SP or SD-RD plane and contains the F, J, $\bar{J}$, E and $\bar{E}$ components. The second fibre is {hkl} ⟨111⟩ and contains D_1, D_2, E and $\bar{E}$ components. Sometimes, the J, $\bar{J}$, E and $\bar{E}$ orientations are labelled as J_1, J_2, E_1 and E_2, respectively [35, 36]. Contrarily to FCC materials, only limited investigations on the evolution of BCC materials after HPT processing are available at present.

The ideal HPT orientations for FCC and BCC materials are overlaid on the experimental data in the ODF sections at φ_2 = 0 and 45° in figure 8 and their characteristics are summarized in Tables 1 and 2.

<Table 1>

<Table 2>

3.4 XRD and hardness analysis of the CuCr alloy after HPT processing and annealing

<Figure 10>

<Table 3>

The XRD patterns of the samples before and after HPT up to N=20 turns are presented in Fig. 10. The patterns of the remaining states (N=5 and HPT + annealing for 1 hour at 210, 550 and 850°C) are not shown since they have the same characteristics. The first point to be noted is the presence of the characteristic peaks of the Cu and Cr phases and a shift of the $(111)_{Cu}$ and $(110)_{Cr}$ BCC phase peaks towards higher Bragg angles and the second point is the reduction of the peak intensity of the former while that of the latter increased. This peak shift may be due to a complicated concomitant causes such as stacking faults, residual strain, grains and sub-grain boundaries [37]. The relative intensity ratio of (110) bcc increased and this is associated with some degree of incorporation of immiscible solutes into the BCC phase and the formation of a supersaturated solid solution in the Cr crystallites [10, 15, 17]. According to another report [19], the estimated value of supersaturation in super saturated solid solutions (SSSSs) of Cu in the

body-centered cubic (bcc) during HPT deformation reaches a maximum of 15 at.% (17.7 wt.%) but there is no formation of SSSSs in the face-centred cubic phase.

The lattice parameters of Cu and Cr before and after HPT and thermal annealing are shown in Table 3. Nominal lattice parameters of Cu and Cr phases are 0.36130 nm (JCPD 03-065-9026) and 0.28839 nm (JCPD 00-006-0694), respectively. The lattice parameter of the Cu phase appears to remain constant after HPT and even after annealing while that of the Cr crystallites increases from 0.28874 to 0.28904 nm after HPT. This increase may be attributed to the formation of a supersaturated solid solution in the BCC phase. The decrease of this parameter after thermal annealing is very plausibly due to a partial decomposition of the previously formed solid solution.

<Figure 11>

Figure 11 presents the evolution of the dislocation density and the mean crystallite size of the Cu43%Cr alloy after HPT processing and annealing. These microstructural parameters have been estimated from the methods described in the "Experimental material and procedures" section.

<Figure 12>

Fig. 12 shows the measured average values of the microhardness recorded near the mid-radius of each disk after HPT processing and annealing the immiscible Cu43%Cr alloy up to 5 and 20 turns and annealing. It is obvious that there is a very significant evolution in the microhardness values after processing by HPT up to 20 turns while the evolution is less pronounced after N=5 turns. Indeed, after 20 turns the microhardness at the mid-radius of the disk (r = R/2) (~ 380 Hv) increases by a factor of approximately 3.5 (relatively to the as-received state) while only by a factor 2.4 after 5 turns without saturation. These results are consistent with those of Guo et al [10] who found that a minimum of about 30 revolutions is needed to achieve a reasonable saturation in hardness across HPT disks of the immiscible Cu43Cr alloy.

The evolution of the hardness after HPT processing up to 20 turns and annealing is surprisingly quite different. It is characterized by an unusual increase (+25%) upon annealing at 210 and 550°C while it is reduced (-40) after annealing at 850°C. Annealing at 210 and 550°C the HPT (N=20) samples caused a moderate hardening of the material. This hardening has already been evidenced in many immiscible alloys (Cu-X, X = Fe, Ag, Co etc..) [38]. Following Kormout et al. [38], the exact mechanisms of this hardening have not been clarified. After annealing at 850°C, the softening is indubitably ascribed to the recovery process.

4. Discussion

The EBSD results in Fig. 4 and 5 evidence a strong refinement of both phases of the immiscible Cu43%Cr alloy after HPT processing up to N= 20 turns. Indeed, a substantial small size is achieved and seems to be identical in both Cu and Cr phases.

There are several reports confirming the greater grain refinement that may be achieved in high purity Cr by comparison with high purity Cu after HPT processing. For example, a report on Cu processed by HPT under a pressure of 6.0 GPa at room temperature showed grain refinement to a size of 280 nm after 10 turns [39] whereas similar experiments on Cr using the same pressure and temperature gave a grain size of 200 nm after only 4 turns [40].

Edalati et al. [41] analyzed the parameters influencing the steady-state grain size of pure metals processed by HPT. The correlations between the steady-state grain size and the physical properties of metals were examined and it was found that the atomic bond energy and the homologous temperature are important parameters influencing the steady-state grain size after processing by HPT. These authors concluded that the steady state grain size tends to decrease with an increase in the shear modulus and this may plausibly explain the greater grain refinement in the Cr phase (G = 115.4 GPa) than in the Cu phase (G = 46.0 GPa) .

The grain microstructure becomes more uniform with increasing HPT turns for both phases. Annealing at 210°C (not shown), 550°C and up to 850°C for one hour did not significantly alter the microstructure. Therefore, any trace of recrystallization or grain growth is noticeable even after high temperature annealing. These results surprisingly show that the as-deformed Cu43%Cr alloy exhibits sufficient thermal stability that it withstands recrystallization and subsequent grain growth during annealing.

As surprisingly shown in Fig. 6, the HAGB values seem to evolve very slightly and especially after N=20 HPT turns and annealing. It is noted that ECAP processing of IF-steel and iron-chromium alloys using route Bc up to 6 and 8 passes resulted in an HAGB fraction close to 60 and 75 %, respectively [42, 43]. It is well known that during the early stages of processing in FCC and BCC materials the microstructure contains a large fraction of LAGBs and these boundaries transform into HAGBs with increasing strain [44]. Such observations have also already been reported [13] where it was concluded from a similar EBSD-OIM analysis that HPT nickel has a significantly larger fraction of high-angle boundaries (68.1%) by comparison with a pure nickel sample (60%) processed by ECAP. However, it is evident from Fig. 7 that there remains a large fraction of LAGB in HPT disks even after processing up to 20 turns.

Similar observations were reported for high purity Al [45], Al–1% Mg solid solution alloy [46] and Al–Li–Mg–Sc alloy [47] after ECAP processing up to 12 passes. These authors ascribed the excess of low-angle boundaries to the continuous introduction of dislocations when processing through repetitive passes in the ECAP die. Kherredine et al [30] reported similar evolution of the grain boundary misorientations in a Cu–2.5%Ni–0.6%Si (wt.%) alloy during processing by HPT at room temperature up to a maximum of 10 turns. Indeed, these authors described a persistent large fraction of low-angle boundaries. It may be assumed that the same mechanism of continuous dislocation generation may operate when processing by ECAP or HPT techniques.

After thermal annealing (Figure 6a) of the N=5 sample, the Cu and Cr HAGB fractions experienced opposite trends. While that of Cu decreased to 63%, the fraction of HAGB in the Cr phase increased to 53%. Annealing the N=20 samples, the HAGB fraction increased to 60-65% and appeared to level off for both phases. This increase is generally explained by the dislocation and low-angle grain boundary annihilation. [48].

The existence of large fractions of low-angle boundaries has often been reported in different materials processed by several SPD techniques [30, 45, 49]. After annealing, neither the histograms of the Cu phase nor those of the Cr phase show an evolution towards misorientation randomization given by the solid line which corresponds to the statistical prediction for a set of random misorientations [50, 51]. Hence, the grain boundary misorientation distributions confirm the persistence of a deformed substructure by the presence of LAGBs even after annealing at 850°C for one hour for the Cu43%Cr alloy. Moreover, the presence of the Cu/Cr interphase boundaries in the alloy should be taken into account. The histogram of the misorientation associated with these interphase boundaries (not presented here) resembles to that of random misorientations and does not show any evolution upon HPT processing and annealing. It is worth noting that such interphase boundaries cannot be described in the terms of misorientations and their effect on the mechanical properties is quite similar to the high-angle grain boundaries [52].

As confirmed by Fig.8 and 9, the textures of the Cu43%Cr alloy after processing by HPT and annealing are fully characterized by the C and weak B orientations in the Cu phase and only by the F orientation in the Cr phase. The texture intensity in the Cu phase increased from 2.91 to 9.94 mrd while that of the Cr phase shows an inverse trend (6.86 to 4.25 mrd) after 5 and 20 HPT turns. Therefore, the texture stabilizes around the main above-cited components although some fluctuations in their positions are evident.

Post HPT annealing did not alter the texture and only some small fluctuations in the intensity is noticed. In general, the evolution of the texture during annealing depends on the phase transformations that may occur after annealing and especially recrystallization and in the present study this phenomenon is absent in both the Cu and Cr phases.

The textures in the present study are composed of C and B orientations of the B fibre (<110> // SD) for Cu and an F orientation which belong to the {110}//SP fibre for Cr. These texture features appear to be quite distinct from those reported for nominally pure Cu or Cu-based alloys and composites deformed by HPT [14] and those expected for BCC elements or alloys such as Fe-Cr [36] and Ta [53] deformed by simple shear.

Indeed, pure Cu often exhibits a weak A-fibre and strong B-fibre with the domination of B/$\overline{\text{B}}$ (ε_{eq} = 127) [54] or presence of A and B fibres and weak C (ε_{eq} = 22.6–113) [55]. For Cu-based alloys with small additions and in a solid solution initial state, there is evidence for the presence of A and B fibres with domination of A_2^* and B/$\overline{\text{B}}$ in Cu-Cr (ε_{eq} = 29) alloys [56] while another report showed A-fibre with the domination of A_2^* in a CuNiSi alloy (ε_{eq} = 101–203) [30]. However, there appears to be no report of the texture evolution in a Cu-based immiscible composite alloy.

There is a report of some textural evolution in nanolayered Cu49%Nb composites fabricated by ARB using Cu and Nb of 99.99% and 99.97% purity elements and then subjected to high pressure torsion [6]. When a large shear strains was applied (0.13, 0.58, 5 and 20 turns), it was reported that the texture in the Cu phase contained an A-fibre mainly around A/$\overline{\text{A}}$ (corresponding to $\{1\bar{1}1\}<110>$ and $\{\bar{1}1\bar{1}\}<\bar{1}\bar{1}0>$) and A_1^*/A_2^* (corresponding to $\{11\bar{1}\}<112>$ and $\{11\bar{1}\}<2\bar{1}1>$). This report noted also that the intensity of the texture components increases with increasing applied strain and the Nb layers showed a tendency towards randomization of the inherited initial ARB texture. These earlier results [6] as well as the present data suggests that the texture evolution of immiscible UFG or nanostructured

hybride systems is strongly influenced by the constraints imposed by the 3-D nanoscale phase co-existence, by the deformation path and also by the initial texture.

The thermal stability and the evolution of mechanical properties after isothermal or isochronal annealing of HPT-processed FCC metals and alloys have been extensively reported but there is only very little information available concerning the recrystallization texture in HPT-processed Ni alloys [57, 58]. Furthermore, the texture development in SPD-deformed Cr alloys has never been reported to date.

It has been reported in a comprehensive review [14] that most of the HPT processing of BCC materials was carried out at high temperatures [36, 59] and/or the texture evolution was investigated as a function of increasing deformation temperature [60, 61]. This is mostly due to the brittle character of these materials which is associated with the lack of easy dislocation movement at low deformation temperatures. Under these high temperature processing conditions, dynamic recrystallization and phase transformations play an progressively significant role during the texture development [60, 61]. Processing at RT leads to the development of all shear components (the F, J, $\bar{J}$, E, $\bar{E}$, D_1 and D_2 components) which is labelled as a typical shear texture in BCC materials while at high deformation temperatures an Oblique Cube component dominates the texture with a weak F component. In the present study, only a unique F orientation was present among the six potential orientations. The Oblique Cube component is a Cube component that undergoes a rotation around the radial direction and then develops through discontinuous dynamic recrystallization [62].

Interestingly, the main component detected is F = {110}<100> which is typical for ordered metals with B2 structure such as NiMnGa [63]. The origin of this component may be associated with the supersaturated solid solution with B2 structure since the Cu atoms occupy the centre of that formed as will be shown via the XRD results in section 3.4 and as stated in other reports [7, 10, 18 ,19].

Contrary to the grain size, which presents a constant evolution with thermal annealing as shown in Fig. 6, the mean crystallite size exhibits a noticeable evolution as in Fig.11 and there is a similar evolution for both Cu and Cr upon HPT processing and annealing. Indeed, the size decreases from N=0 to N=5 and N=20 and increases after annealing. A slight difference is evident and this is because the crystallite size began to increase soon after annealing at 210°C in the N=20 turns while for N=5 it increased only slightly. The dislocation densities have the same evolution for the two phases. After N=5 the density considerably increases after N=5 for the Cr phase but more modestly for the Cu phase and then decreases for both phases. Surprisingly, after N=20 HPT turns and subsequent annealing the evolutions are similar such that the plots can be superimposed. It is worth noting that dislocation density values are ten times lower than those estimated in another report from TEM measurements [17]. It seems probable that the values reported by TEM are overestimates since dislocations densities in the range of ~10^{16} m^{-2} are seldom reported. However, the present values are consistent with the available published data for Cu-based alloys processed by SPD [64, 65].

It is important to also consider some pertinent details about the differences in the values of the grain sizes measured by the EBSD, TEM and XRDLPA techniques. In general, EBSD data collection and analysis are based on the definition of a “grain” which is a continuous set of pixels in space and therefore there are dedicated algorithm groups of connected and similarly oriented points that constitute "grains". This means that an EBSD map is a virtual transcription of real microstructural features under well-defined conditions [66].

In the literature of XRDLPA, the “apparent” average crystallite size in the direction of the diffraction vector is also called the “column length” following an earlier definition [67]. The concept of column length ideally considers grains in a polycrystalline system as made of a column of cells along the scattering direction. Even at large misorientation angles, the subgrains seem to be separated by layers of finite thickness, which may be more accurately described as arrangements of dislocations. Therefore, it is only after deformation at elevated temperatures or after subsequent annealing that grain boundaries in the classical sense are observed [68].

Indeed, it was stated that in an alloy of medium or high stacking fault energy (SFE) the dislocations are classically organized after deformation in the form of a three-dimensional cell structure [69]. After subsequent annealing, owing to recovery the tangled cell walls transform to more regular dislocation networks or low-angle grain boundaries and the number of dislocations in the cell interiors also weakens. The cells therefore become subgrains and at this scale they be can well observed by TEM. There is a published analysis of the microstructure of an ARMCO iron processed by 16 ECAP passes via EBSD, TEM and XRDLPA (MAUD for Material Analysis Using Diffraction) [70]. It was demonstrated that quite different values of grain, sub-grain and crystallite sizes were obtained using each technique. Thus, the lower values were obtained by XRDLPA whereas two to three times higher values were achieved by TEM or EBSD techniques, respectively.

The hardness values consigned in Figure 12 are higher than those reported earlier for pure Cu (N=5) [71, 72], Cu–0.1% Zr (N=5) [73, 74], Cu–1.5% Si [75], Cu-2.5Ni-0.6Si [76]. Measurements on a Cu–28% Ag alloy gave an approaching hardness of Hv≈350 after HPT for 10 turns [77]. Annealing the HPT (N=5) processed discs gave a gradual softening of the material due to the occurrence of a recovery phenomenon without recrystallization which is indicated by the absence of a strong grain size change and crystallographic texture. This assumption is also supported by the global evolution of the crystallite size and dislocation density. This

subsequent strong softening corresponds to a total recovery of the microstructure without recrystallization.

It is well known that the global hardness after SPD processing is mainly due to the grain refinement via grain boundary hardening governed by the Hall-Petch relation ($Hv \sim d^{-0.5}$ [78]) and dislocation accumulation through work hardening which follows the equation ($Hv \sim (\rho)^{0.5}$ [79].

However, it was suggested that an increase of the hardness may also probably be caused by an increase in the number of microvoids [80], which represent obstacles for the movement of dislocations. It is then reasonable to assume that the global hardening of the Cu43%Cr after HPT processing up to 5 and 20 turns is caused by the grain refinement, by the dislocation density increasing and by vacancy cluster (microvoids) creation. After annealing, the grain size appears stable while the dislocation density falls close to the initial value of the as-received material.

The global evolution of the crystallite size and dislocation density suggests the occurrence of a recovery phenomenon without recrystallization which is indicated by the absence of a strong grain size change and texture as discussed earlier. The drop of the dislocation density is monotonous and it reaches the value of the initial un-processed material.

Recovery without recrystallization is inferred due to the reduced mobility of the grain boundaries and the inhibition of their motion. The reduction in their mobility is explained by two main methods: the so-called kinetic approach or the driving force in the so-called thermodynamic approach. In the first case, a variety of "tracks" including nano-inclusions, nanopores, Zener pinning, triple junctions, and quadruple points can slow or stop grain boundary mobility [26]. In the second method, solute segregation decreases the energy at grain boundaries. These two methods are closely related in general.

The thermal stability at high temperatures of immiscible alloys, with a low percentage of secondary phases (<20%), [25, 81, 82, 83], is generally based on Zener pinning which is very effective in the case of particles of small size and large volume fractions and/or by solute segregation to grains boundaries. This does not hold in the present study because of the clear and established thermal stability of the microstructure. However, the main cause of the reduction of the grain boundary mobility in the present investigation is explained by the forced intermixing of the Cu and Cr after HPT processing. Indeed, this intermixing with the formation of SSSS has been discussed based on the fragmentation process of Cu grains [19]. The fragmentation behaviour of the Cr particles in the Cu–Cr composite during deformation resembles that of the W–Cu composite material [84].

It is assumed that the refinement of the Cr particles was continuous until reaching a limit of around 10 nm [19, 85]. Beneath this cut off, Cr particles may be steadily flattened, fractured and re-bonded as in the ball milling process [19, 85]. Hence, SPD can cause a forced intermixing between Cu and Cr grains with Cu atoms dissolved into the Cr matrix in the form of solutes or clusters [10, 15]. These clusters will undoubtedly hinder the motion of the grain boundaries in the framework of the first above-cited approach called the kinetic model.

Generally, grain coarsening is required for grain growth and atom transfer between phases is required. However, such a diffusion process is very slow in immiscible alloys due to the limited solubility of individual elements in the solid state, even at high temperatures (usually up to the melting temperature).

Quite a similar thermal stability to that evident in the present study was reported in an HPT-processed Cu-50%.at Ta alloy [86]. This enhanced thermal stability was attributed to a Cu-Ta solid solution formation and dispersion of fine Ta nano-particles inside the Cu-rich grains which effectively hinders dislocation and grain boundary motion. Moreover, bright field transmission

electron microscopy patterns confirmed the existence of nanoclusters of Cu in the Cr phase in the HPT-processed Cu43%Cr alloy which also explains its stability [17].

Comparable results were obtained for an immiscible mechanically-alloyed and spark plasma sintering (SPS) Cu50(FeCo)50 immiscible alloy [87]. Subsequent annealing for 3 h at 800 and 980 °C showed that the alloy exhibited excellent thermal stability and this stability was explained by the immiscible nature of Cu-Fe based alloys.

Finally, the mean grain size from EBSD measurements, crystallite size from XRDLPA analysis and the dislocation density evolution are all against the occurrence of recrystallization and/or grain growth and they are consistent with the considerable thermal stability of the Cu-43Cr alloy processed by HPT.

5. Summary and conclusions

Experiments were conducted to examine the influence of high-pressure torsion processing and annealing on microstructure, texture and thermal stability of an immiscible composite Cu-43Cr (wt.%) alloy using electron backscatter diffraction, X-ray diffraction and microhardness measurements. The results show that the Cu and Cr grains were refined down to 0.45 and 0.39 μm, respectively, with equiaxed morphologies. The crystallographic texture was dominated by a shear type orientations labelled C in Cu and F in the Cr phases. The ultrafine-grained microstructure and texture of the Cu43%Cr composite alloy were retained surprisingly up to 850 °C. The dislocation densities in Cu and Cr phases increased by one decade (~ 1.1 and 2.4 10^{15} m^{-2}, respectively) after HPT processing and dropped close to the initial value of the as-received and undeformed sample (~ 2.5 10^{14} m^{-2}) after annealing up to 850°C. The global results show that the immiscible composite exhibits a high thermal stability up to the temperate of 850°C. The evolution of the microstructure, texture, dislocations density and crystallite size of the UFG Cu43%Cr alloy suggest a recovery mechanism without recrystallization.

Declaration of interests

The authors declare that they have no known competing financial interests or personal relationships that could have appeared to influence the work reported in this paper.

Acknowledgement

The work of two of the authors was supported by the European Research Council under Grant Agreement No. 267464-SPDMETALS (YH and TGL).

References

[1] L.-M. Peng, X.-M. Mao, K.-D. Xu, et W.-J. Ding, « Property and thermal stability of in situ composite Cu–Cr alloy contact cable », Journal of Materials Processing Technology, vol. 166, no 2, p. 193-198, août 2005, doi: 10.1016/j.jmatprotec.2004.08.013.

[2] X. Sun, J. Jie, T. Wang, et T. Li, « Effect of two-step cryorolling and aging on mechanical and electrical properties of a Cu–Cr–Ni–Si alloy for lead frames applications », Materials Science and Engineering: A, vol. 809, p. 140521, mars 2021, doi: 10.1016/j.msea.2020.140521.

[3] H. Kojima et al., « Conditioning mechanism of Cu-Cr electrode based on electrode surface state under impulse voltage application in vacuum », IEEE Trans. Dielect. Electr. Insul., vol. 18, no 6, p. 2108-2114, déc. 2011, doi: 10.1109/TDEI.2011.6118651.

[4] Ph. Kiryukhantsev-Korneev et al., « Hard Wear-Resistant Ti-Si-C Coatings for Cu-Cr Electrical Contacts », Materials, vol. 16, no 3, p. 936, janv. 2023, doi: 10.3390/ma16030936.

[5] R. Z. Valiev, R. K. Islamgaliev, et I. V. Alexandrov, « Bulk nanostructured materials from severe plastic deformation », Progress in Materials Science, vol. 45, no 2, p. 103-189, mars 2000, doi: 10.1016/S0079-6425(99)00007-9.

[6] E. H. Ekiz et al., « Microstructural evolution of nanolayered Cu–Nb composites subjected to high-pressure torsion », Acta Materialia, vol. 72, p. 178-191, juin 2014, doi: 10.1016/j.actamat.2014.03.040.

[7] J. Guo et al., « In situ atomic-scale observation of oxidation and decomposition processes in nanocrystalline alloys », Nat Commun, vol. 9, no 1, p. 946, mars 2018, doi: 10.1038/s41467-018-03288-8.

[8] T. Mousavi et al., « Fabrication and characterization of nanostructured immiscible Cu–Ta alloys processed by high-pressure torsion », Journal of Alloys and Compounds, vol. 832, p. 155007, août 2020, doi: 10.1016/j.jallcom.2020.155007.

[9] D. Luo, T. Huminiuc, Y. Huang, T. Polcar, et T. G. Langdon, « fabricationThe of high strength Zr/Nb nanocomposites using high-pressure torsion », Materials Science and Engineering: A, vol. 790, p. 139693, juill. 2020, doi: 10.1016/j.msea.2020.139693.

[10] J. Guo, J. M. Rosalie, R. Pippan, et Z. Zhang, « Revealing the Microstructural evolution in Cu-Cr nanocrystalline alloys during high pressure torsion », Materials Science and Engineering: A, vol. 695, p. 350-359, mai 2017, doi: 10.1016/j.msea.2017.04.034.

[11] R. Z. Valiev et T. G. Langdon, « Principles of equal-channel angular pressing as a processing tool for grain refinement », Progress in Materials Science, vol. 51, no 7, p. 881-981, sept. 2006, doi: 10.1016/j.pmatsci.2006.02.003.

[12] S. M. Ghalehbandi, M. Malaki, et M. Gupta, « Accumulative Roll Bonding—A Review », Applied Sciences, vol. 9, no 17, p. 3627, sept. 2019, doi: 10.3390/app9173627.

[13] A. P. Zhilyaev et T. G. Langdon, « Using high-pressure torsion for metal processing: Fundamentals and applications », Progress in Materials Science, vol. 53, no 6, p. 893-979, août 2008, doi: 10.1016/j.pmatsci.2008.03.002.

[14] H. Azzeddine, D. Bradai, T. Baudin, et T. G. Langdon, « Texture evolution in high-pressure torsion processing », Progress in Materials Science, vol. 125, p. 100886, avr. 2022, doi: 10.1016/j.pmatsci.2021.100886.

[15] J. Guo, J. Rosalie, R. Pippan, et Z. Zhang, « On the phase evolution and dissolution process in Cu-Cr alloys deformed by high pressure torsion », Scripta Materialia, vol. 133, p. 41-44, mai 2017, doi: 10.1016/j.scriptamat.2017.02.009.

[16] J. Guo et al., « Combined Fe and O effects on microstructural evolution and strengthening in Cu–Fe nanocrystalline alloys », Materials Science and Engineering: A, vol. 772, p. 138800, janv. 2020, doi: 10.1016/j.msea.2019.138800.

[17] Q. Shao, J. Guo, J. Chen, et Z. Zhang, « Atomic-scale investigation on the structural evolution and deformation behaviors of Cu–Cr nanocrystalline alloys processed by high-pressure torsion », Journal of Alloys and Compounds, vol. 832, p. 154994, août 2020, doi: 10.1016/j.jallcom.2020.154994.

[18] X. Sauvage, P. Jessner, F. Vurpillot, et R. Pippan, « Nanostructure and properties of a Cu–Cr composite processed by severe plastic deformation », Scripta Materialia, vol. 58, no 12, p. 1125-1128, juin 2008, doi: 10.1016/j.scriptamat.2008.02.010.

[19] A. Bachmaier, G. B. Rathmayr, M. Bartosik, D. Apel, Z. Zhang, et R. Pippan, « New insights on the formation of supersaturated solid solutions in the Cu–Cr system

deformed by high-pressure torsion », Acta Materialia, vol. 69, p. 301-313, mai 2014, doi: 10.1016/j.actamat.2014.02.003.

[20] Z. Zhang, J. Guo, G. Dehm, et R. Pippan, « In-situ tracking the structural and chemical evolution of nanostructured CuCr alloys », Acta Materialia, vol. 138, p. 42-51, oct. 2017, doi: 10.1016/j.actamat.2017.07.039.

[21] M. J. Zehetbauer et Y. T. Zhu, Éd., Bulk Nanostructured Materials, 1re éd. Wiley, 2009. doi: 10.1002/9783527626892.

[22] P. Jenei, J. Gubicza, E. Y. Yoon, H. S. Kim, et J. L. Lábár, « High temperature thermal stability of pure copper and copper–carbon nanotube composites consolidated by High Pressure Torsion », Composites Part A: Applied Science and Manufacturing, vol. 51, p. 71-79, août 2013, doi: 10.1016/j.compositesa.2013.04.007.

[23] Z. Hegedűs, J. Gubicza, M. Kawasaki, N. Q. Chinh, J. L. Lábár, et T. G. Langdon, « Stability of the ultrafine-grained microstructure in silver processed by ECAP and HPT », J Mater Sci, vol. 48, no 13, p. 4637-4645, juill. 2013, doi: 10.1007/s10853-012-7124-5.

[24] G. Wilde et H. Rösner, « Stability aspects of bulk nanostructured metals and composites », J Mater Sci, vol. 42, no 5, p. 1772-1781, mars 2007, doi: 10.1007/s10853-006-0986-7.

[25] C. C. Koch, R. O. Scattergood, M. Saber, et H. Kotan, « High temperature stabilization of nanocrystalline grain size: Thermodynamic versus kinetic strategies », J. Mater. Res., vol. 28, no 13, p. 1785-1791, juill. 2013, doi: 10.1557/jmr.2012.429.

[26] R. A. Andrievski, « Review of thermal stability of nanomaterials », J Mater Sci, vol. 49, no 4, p. 1449-1460, févr. 2014, doi: 10.1007/s10853-013-7836-1.

[27] L. Lutterotti, S. Matthies, H.-R. Wenk, A. S. Schultz, et J. W. Richardson, « Combined texture and structure analysis of deformed limestone from time-of-flight neutron diffraction spectra », Journal of Applied Physics, vol. 81, no 2, p. 594-600, janv. 1997, doi: 10.1063/1.364220.

[28] G. K. Williamson et R. E. Smallman, « III. Dislocation densities in some annealed and cold-worked metals from measurements on the X-ray debye-scherrer spectrum », Philosophical Magazine, vol. 1, no 1, p. 34-46, janv. 1956, doi: 10.1080/14786435608238074.

[29] F. J. Humphreys, « Review Grain and subgrain characterisation by electron backscatter diffraction », Journal of Materials Science, vol. 36, no 16, p. 3833-3854, 2001, doi: 10.1023/A:1017973432592.

[30] A. Y. Khereddine et al., « Microstructures and textures of a Cu–Ni–Si alloy processed by high-pressure torsion », Journal of Alloys and Compounds, vol. 574, p. 361-367, oct. 2013, doi: 10.1016/j.jallcom.2013.05.051.

[31] K. Abib, J. A. M. Balanos, B. Alili, et D. Bradai, « On the microstructure and texture of Cu-Cr-Zr alloy after severe plastic deformation by ECAP », Materials Characterization, vol. 112, p. 252-258, févr. 2016, doi: 10.1016/j.matchar.2015.12.026.

[32] K. Tirsatine et al., « Texture and microstructure evolution of Fe–Ni alloy after accumulative roll bonding », Journal of Alloys and Compounds, vol. 610, p. 352-360, oct. 2014, doi: 10.1016/j.jallcom.2014.04.173.

[33] G. R. Canova, U. F. Kocks, et J. J. Jonas, « Theory of torsion texture development », Acta Metallurgica, vol. 32, no 2, p. 211-226, févr. 1984, doi: 10.1016/0001-6160(84)90050-6.

[34] F. Montheillet, P. Gilormini, et J. J. Jonas, « Relation between axial stresses and texture development during torsion testing: A simplified theory », Acta Metallurgica, vol. 33, no 4, p. 705-717, avr. 1985, doi: 10.1016/0001-6160(85)90035-5.

[35] Y. Zhao, R. Massion, T. Grosdidier, et L. S. Toth, « Gradient Structure in High Pressure Torsion Compacted Iron Powder: Gradient Structure in High Pressure Torsion… », Adv. Eng. Mater., vol. 17, no 12, p. 1748-1753, déc. 2015, doi: 10.1002/adem.201500012.

[36] J. Duan, H. Wen, C. Zhou, R. Islamgaliev, et X. Li, « Evolution of microstructure and texture during annealing in a high-pressure torsion processed Fe-9Cr alloy », Materialia, vol. 6, p. 100349, juin 2019, doi: 10.1016/j.mtla.2019.100349.

[37] T. Ungár, « Microstructural parameters from X-ray diffraction peak broadening », Scripta Materialia, vol. 51, no 8, p. 777-781, oct. 2004, doi: 10.1016/j.scriptamat.2004.05.007.

[38] K. S. Kormout, R. Pippan, et A. Bachmaier, « Deformation-Induced Supersaturation in Immiscible Material Systems during High-Pressure Torsion », Adv Eng Mater, vol. 19, no 4, p. 1600675, avr. 2017, doi: 10.1002/adem.201600675.

[39] A. I. Almazrouee, K. J. Al-Fadhalah, S. N. Alhajeri, et T. G. Langdon, « Microstructure and microhardness of OFHC copper processed by high-pressure torsion », Materials Science and Engineering: A, vol. 641, p. 21-28, août 2015, doi: 10.1016/j.msea.2015.06.016.

[40] S. Lee et Z. Horita, « High-Pressure Torsion for Pure Chromium and Niobium », Mater. Trans., vol. 53, no 1, p. 38-45, 2012, doi: 10.2320/matertrans.MD201131.

[41] K. Edalati et Z. Horita, « Parameters Influencing Steady-State Grain Size of Pure Metals Processed by High-Pressure Torsion », MSF, vol. 706-709, p. 3034-3039, janv. 2012, doi: 10.4028/www.scientific.net/MSF.706-709.3034.

[42] A. A. Gazder, W. Cao, C. H. J. Davies, et E. V. Pereloma, « An EBSD investigation of interstitial-free steel subjected to equal channel angular extrusion », Materials Science and Engineering: A, vol. 497, no 1-2, p. 341-352, déc. 2008, doi: 10.1016/j.msea.2008.07.030.

[43] M. Rifai et H. Miyamoto, « Effect of strain energy on the grain growth behaviour of ultrafine-grained iron-chromium alloy by equal channel angular pressing », JMES, vol. 14, no 3, p. 7049-7057, sept. 2020, doi: 10.15282/jmes.14.3.2020.07.0552.

[44] K. S. Suresh, S. Sinha, A. Chaudhary, et S. Suwas, « Development of microstructure and texture in Copper during warm accumulative roll bonding », Materials Characterization, vol. 70, p. 74-82, août 2012, doi: 10.1016/j.matchar.2012.04.017.

[45] M. Kawasaki, Z. Horita, et T. G. Langdon, « Microstructural evolution in high purity aluminum processed by ECAP », Materials Science and Engineering: A, vol. 524, no 1-2, p. 143-150, oct. 2009, doi: 10.1016/j.msea.2009.06.032.

[46] C. Xu, Z. Horita, et T. G. Langdon, « Microstructural evolution in an aluminum solid solution alloy processed by ECAP », Materials Science and Engineering: A, vol. 528, no 18, p. 6059-6065, juill. 2011, doi: 10.1016/j.msea.2011.04.017.

[47] R. Kaibyshev, K. Shipilova, F. Musin, et Y. Motohashi, « Continuous dynamic recrystallization in an Al–Li–Mg–Sc alloy during equal-channel angular extrusion », Materials Science and Engineering: A, vol. 396, no 1-2, p. 341-351, avr. 2005, doi: 10.1016/j.msea.2005.01.053.

[48] K. Tirsatine et al., « An EBSD analysis of Fe-36%Ni alloy processed by HPT at ambient and a warm temperature », Journal of Alloys and Compounds, vol. 753, p. 46-53, juill. 2018, doi: 10.1016/j.jallcom.2018.04.194.

[49] A. Loucif, R. B. Figueiredo, T. Baudin, F. Brisset, et T. G. Langdon, « Microstructural Evolution in an Al-6061 Alloy Processed by High-Pressure Torsion and Rapid Annealing », MSF, vol. 667-669, p. 223-228, déc. 2010, doi: 10.4028/www.scientific.net/MSF.667-669.223.

[50] A. Garbacz et M. W. Grabski, « Modelling of CSL boundaries distribution in polycrystals », Scripta Metallurgica, vol. 23, no 8, p. 1369-1374, août 1989, doi: 10.1016/0036-9748(89)90061-6.

[51] D. H. Warrington et M. Boon, « Ordered structures in random grain boundaries; some geometrical probabilities », Acta Metallurgica, vol. 23, no 5, p. 599-607, mai 1975, doi: 10.1016/0001-6160(75)90100-5.

[52] S. V. Zherebtsov, G. A. Salishchev, R. M. Galeyev, O. R. Valiakhmetov, S. Yu. Mironov, et S. L. Semiatin, « Production of submicrocrystalline structure in large-scale Ti–6Al–4V billet by warm severe deformation processing », Scripta Materialia, vol. 51, no 12, p. 1147-1151, déc. 2004, doi: 10.1016/j.scriptamat.2004.08.018.

[53] A. Panigrahi et al., « Mechanical properties, structural and texture evolution of biocompatible Ti–45Nb alloy processed by severe plastic deformation », Journal of the Mechanical Behavior of Biomedical Materials, vol. 62, p. 93-105, sept. 2016, doi: 10.1016/j.jmbbm.2016.04.042.

[54] N. A. Enikeev, E. Schafler, M. Zehetbauer, I. V. Alexandrov, et R. Valiev, « Observations of Texture in Large Scale HPT-Processed Cu », MSF, vol. 584-586, p. 367-374, juin 2008, doi: 10.4028/www.scientific.net/MSF.584-586.367.

[55] K. J. Al-Fadhalah, S. N. Alhajeri, A. I. Almazrouee, et T. G. Langdon, « Microstructure and microtexture in pure copper processed by high-pressure torsion », J Mater Sci, vol. 48, no 13, p. 4563-4572, juill. 2013, doi: 10.1007/s10853-013-7200-5.

[56] A. Korneva, B. Straumal, A. Kilmametov, R. Chulist, P. Straumal, et P. Zięba, « Phase transformations in a Cu Cr alloy induced by high pressure torsion », Materials Characterization, vol. 114, p. 151-156, avr. 2016, doi: 10.1016/j.matchar.2016.02.017.

[57] B. K. Kim, J. A. Szpunar, et A. P. Zhilyaev, « Annealing Texture in Thermal Stability of Ultrafine-Grained Ni », MSF, vol. 408-412, p. 943-948, août 2002, doi: 10.4028/www.scientific.net/MSF.408-412.943.

[58] H. W. Zhang, X. Huang, R. Pippan, et N. Hansen, « Thermal behavior of Ni (99.967% and 99.5% purity) deformed to an ultra-high strain by high pressure torsion », Acta Materialia, vol. 58, no 5, p. 1698-1707, mars 2010, doi: 10.1016/j.actamat.2009.11.012.

[59] Y. Wang et J. Aktaa, « Microstructural evolution, textural evolution and thermal stabilities of W and W – 1 wt% La2O3 subjected to high-pressure torsion », Materialia, vol. 2, p. 46-52, oct. 2018, doi: 10.1016/j.mtla.2018.05.009.

[60] R. Chulist, A. Böhm, E. Rybacki, T. Lippmann, C. G. Oertel, et W. Skrotzki, « Texture Evolution of HPT-Processed Ni50Mn29Ga21 », MSF, vol. 702-703, p. 169-172, déc. 2011, doi: 10.4028/www.scientific.net/MSF.702-703.169.

[61] O. Renk, P. Ghosh, et R. Pippan, « Generation of extreme grain aspect ratios in severely deformed tantalum at elevated temperatures », Scripta Materialia, vol. 137, p. 60-63, août 2017, doi: 10.1016/j.scriptamat.2017.04.024.

[62] B. Klöden, C.-G. Oertel, W. Skrotzki, et E. Rybacki, « Microstructure Development During High Strain Torsion of NiAl », Journal of Engineering Materials and Technology, vol. 131, no 1, p. 011101, janv. 2009, doi: 10.1115/1.3030882.

[63] R. Chulist, W. Skrotzki, C.-G. Oertel, A. Böhm, H.-G. Brokmeier, et T. Lippmann, « Cyclic fibre texture in hot extruded Ni 50 Mn 29 Ga 21 », International Journal of Materials Research, vol. 103, no 5, p. 575-579, mai 2012, doi: 10.3139/146.110735.

[64] A. Y. Khereddine, F. H. Larbi, M. Kawasaki, T. Baudin, D. Bradai, et T. G. Langdon, « An examination of microstructural evolution in a Cu–Ni–Si alloy processed by HPT and ECAP », Materials Science and Engineering: A, vol. 576, p. 149-155, août 2013, doi: 10.1016/j.msea.2013.04.004.

[65] K. Abib, F. H. Larbi, L. Rabahi, B. Alili, et D. Bradai, « DSC analysis of commercial Cu–Cr–Zr alloy processed by equal channel angular pressing », Transactions of Nonferrous Metals Society of China, vol. 25, no 3, p. 838-843, mars 2015, doi: 10.1016/S1003-6326(15)63671-8.

[66] Y. Chen, J. Hjelen, et H. J. Roven, « Application of EBSD technique to ultrafine grained and nanostructured materials processed by severe plastic deformation: Sample preparation, parameters optimization and analysis », Transactions of Nonferrous Metals Society of China, vol. 22, no 8, p. 1801-1809, août 2012, doi: 10.1016/S1003-6326(11)61390-3.

[67] E. J. Mittemeijer et P. Scardi, Éd., Diffraction Analysis of the Microstructure of Materials, vol. 68. in Springer Series in Materials Science, vol. 68. Berlin, Heidelberg: Springer Berlin Heidelberg, 2004. doi: 10.1007/978-3-662-06723-9.

[68] N. A. Akhmadeev, N. P. Kobelev, R. R. Mulyukov, Ya. M. Soifer, et R. Z. Valiev, « The effect of heat treatment on the elastic and dissipative properties of copper with the submicrocrystalline structure », Acta Metallurgica et Materialia, vol. 41, no 4, p. 1041-1046, avr. 1993, doi: 10.1016/0956-7151(93)90153-J.

[69] F. J. Humphreys et M. Hatherly, Recrystallization and Related Phenomena. Oxford, Pergamon, 1995.

[70] J. A. Muñoz et al., « Analysis of the micro and substructural evolution during severe plastic deformation of ARMCO iron and consequences in mechanical properties », Materials Science and Engineering: A, vol. 740-741, p. 108-120, janv. 2019, doi: 10.1016/j.msea.2018.10.100.

[71] Z. Horita et T. G. Langdon, « Microstructures and microhardness of an aluminum alloy and pure copper after processing by high-pressure torsion », Materials Science and Engineering: A, vol. 410-411, p. 422-425, nov. 2005, doi: 10.1016/j.msea.2005.08.133.

[72] A. P. Zhilyaev, A. A. Gimazov, G. I. Raab, et T. G. Langdon, « Using high-pressure torsion for the cold-consolidation of copper chips produced by machining », Materials Science and Engineering: A, vol. 486, no 1-2, p. 123-126, juill. 2008, doi: 10.1016/j.msea.2007.08.070.

[73] J. Wongsa-Ngam, M. Kawasaki, Y. Zhao, et T. G. Langdon, « Microstructural evolution and mechanical properties of a Cu–Zr alloy processed by high-pressure torsion », Materials Science and Engineering: A, vol. 528, no 25-26, p. 7715-7722, sept. 2011, doi: 10.1016/j.msea.2011.06.056.

[74] J. Wongsa-Ngam, M. Kawasaki, et T. G. Langdon, « Achieving homogeneity in a Cu–Zr alloy processed by high-pressure torsion », J Mater Sci, vol. 47, no 22, p. 7782-7788, nov. 2012, doi: 10.1007/s10853-012-6587-8.

[75] H. Jiang, Y. T. Zhu, D. P. Butt, I. V. Alexandrov, et T. C. Lowe, « Microstructural evolution, microhardness and thermal stability of HPT-processed Cu », Materials Science and Engineering: A, vol. 290, no 1-2, p. 128-138, oct. 2000, doi: 10.1016/S0921-5093(00)00919-9.

[76] H. Matsunaga, Z. Horita, K. Imamura, T. Kiss, et X. Sauvage, « Aging Behavior of Cu-Ni-Si Alloy Processed by High-Pressure Torsion », MSF, vol. 667-669, p. 307-312, déc. 2010, doi: 10.4028/www.scientific.net/MSF.667-669.307.

[77] Y. Z. Tian, S. D. Wu, Z. F. Zhang, R. B. Figueiredo, N. Gao, et T. G. Langdon, « Strain hardening behavior of a two-phase Cu–Ag alloy processed by high-pressure torsion », Scripta Materialia, vol. 65, no 6, p. 477-480, sept. 2011, doi: 10.1016/j.scriptamat.2011.06.004.

[78] N. J. Petch, « The ductile-brittle transition in the fracture of α-iron: I », Philosophical Magazine, vol. 3, no 34, p. 1089-1097, oct. 1958, doi: 10.1080/14786435808237038.

[79] « The mechanism of plastic deformation of crystals. Part I.—Theoretical », Proc. R. Soc. Lond. A, vol. 145, no 855, p. 362-387, juill. 1934, doi: 10.1098/rspa.1934.0106.

[80] J. Cizek et al., « Ultra Fine Grained Copper Prepared by High Pressure Torsion: Spatial Distribution of Defects from Positron Annihilation Spectroscopy », in Nanomaterials by Severe Plastic Deformation, M. Zehetbauer et R. Z. Valiev, Éd., Weinheim, FRG: Wiley-VCH Verlag GmbH & Co. KGaA, 2005, p. 407-412. doi: 10.1002/3527602461.ch7b.

[81] K. A. Darling, A. J. Roberts, Y. Mishin, S. N. Mathaudhu, et L. J. Kecskes, « Grain size stabilization of nanocrystalline copper at high temperatures by alloying with tantalum », Journal of Alloys and Compounds, vol. 573, p. 142-150, oct. 2013, doi: 10.1016/j.jallcom.2013.03.177.

[82] S. Özerinç, K. Tai, N. Q. Vo, P. Bellon, R. S. Averback, et W. P. King, « Grain boundary doping strengthens nanocrystalline copper alloys », Scripta Materialia, vol. 67, no 7-8, p. 720-723, oct. 2012, doi: 10.1016/j.scriptamat.2012.06.031.

[83] K. A. Darling, L. J. Kecskes, M. Atwater, J. Semones, R. O. Scattergood, et C. C. Koch, « Thermal stability of nanocrystalline nickel with yttrium additions », J. Mater. Res., vol. 28, no 13, p. 1813-1819, juill. 2013, doi: 10.1557/jmr.2013.9.

[84] I. Sabirov et R. Pippan, « Characterization of tungsten fragmentation in a W–25%Cu composite after high-pressure torsion », Materials Characterization, vol. 58, no 10, p. 848-853, oct. 2007, doi: 10.1016/j.matchar.2006.08.001.

[85] S. Romankov, Y. C. Park, I. V. Shchetinin, et J. M. Yoon, « Atomic-scale intermixing, amorphization and microstructural development in a multicomponent system subjected to surface severe plastic deformation », Acta Materialia, vol. 61, no 4, p. 1254-1265, févr. 2013, doi: 10.1016/j.actamat.2012.11.001.

[86] N. Ibrahim, M. Peterlechner, F. Emeis, M. Wegner, S. V. Divinski, et G. Wilde, « Mechanical alloying via high-pressure torsion of the immiscible Cu50Ta50 system », Materials Science and Engineering: A, vol. 685, p. 19-30, févr. 2017, doi: 10.1016/j.msea.2016.12.106.

[87] T. Niu et al., « Texture development in Cu-Ag-Fe triphase immiscible nanocomposites with superior thermal stability », Acta Materialia, vol. 244, p. 118545, janv. 2023, doi: 10.1016/j.actamat.2022.118545.

Figures Captions

Figure 1 : Illustration showing the principles of HPT processing.

Figure 2 : Characteristics of the Cu43%Cr alloy in the as-received state, a) SEM-EBSD patterns in the CD-IPF mode in Cu43%Cr alloy, b) in Cu phase and c) in Cr phase, d) misorientation angle histograms.

Figure 3 : ODF sections of the Cu43%Cr alloy in the as-received state, a) at φ_2 =0, 45 and 65° for the Cu phase, b) at φ_2 =45° for Cr phase.

Figure 4 : Orientation imaging micrographs (CD-IPF mode) of the Cu (left) and Cr (right) in the Cu43%Cr alloy after 5 turns HPT (25°C) and annealing at 550°C and 850°C.

Figure 5 : Orientation imaging micrographs (CD-IPF mode) of the Cu (left) and Cr (right) in the Cu43%Cr alloy after 20 turns HPT (25°C) and annealing at 550°C and 850°C.

Figure 6 : Evolution of the mean grain size and high-angle grain boundary fraction (HAGB) of the Cu43%Cr alloy after HPT processing up to a) N= 5 and b) N=20 HPT turns and annealing.

Figure 7 : Histograms of the grain boundary misorientation angles after HPT processing and annealing of the Cu43%Cr alloy, a) Cu (N=5), b) Cr (N=5), a) Cu (N=20) and d) Cr (N=20) phases.

Figure 8 : ODF section at φ_2 = 0 and 45° of the Cu43%Cr alloy after 5 turns HPT and annealing.

Figure 9 : ODF section at φ_2 = 0 and 45° of the Cu43%Cr alloy after 20 turns HPT and annealing.

Figure 10 : (a) XRD analysis of the Cu43%Cr alloy before and after HPT processing (20 turns) and b) zoom of an area near the $(111)_{Cu}$.

Figure 11 : Evolution of the dislocation density and the mean crystallite size of the Cu43%Cr alloy after HPT processing and annealing.

Figure 12 : Evolution of the global microhardness of the Cu43%Cr alloy after HPT processing and annealing.

Tables Captions

Table 1: Position of ideal shear texture components for FCC metals and alloys projected in SD-RD plane.

Table 2: Position of ideal shear texture components for BCC metals and alloys projected in SD-RD plane.

Table 3: Lattice parameter, crystallite size and dislocations density of Cu and Cr phases in Cu43%Cr alloy after HPT processing and annealing for 1 hour at 210, 550 and 850°C.

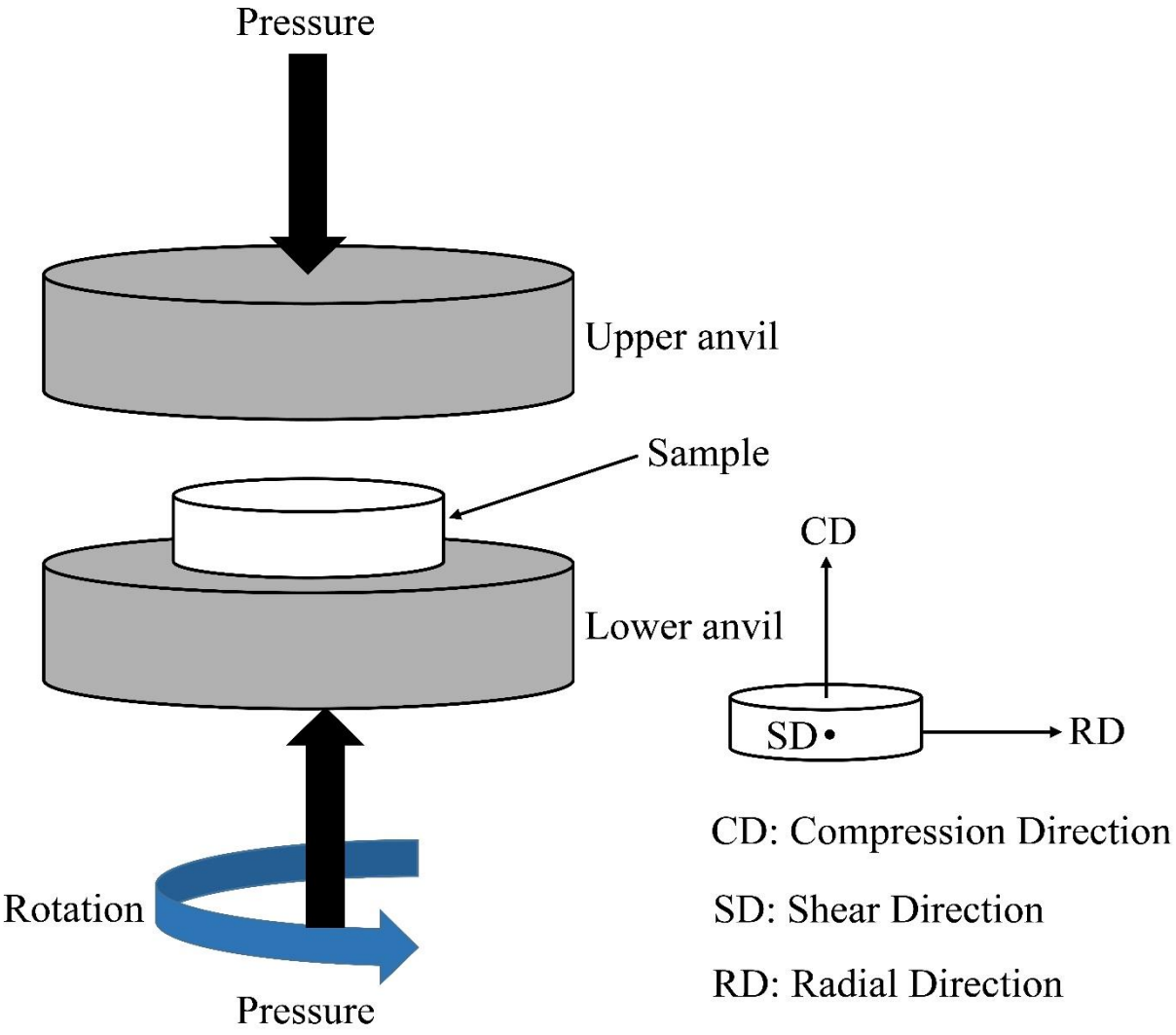

Figure 1: Illustration showing the principles of HPT processing.

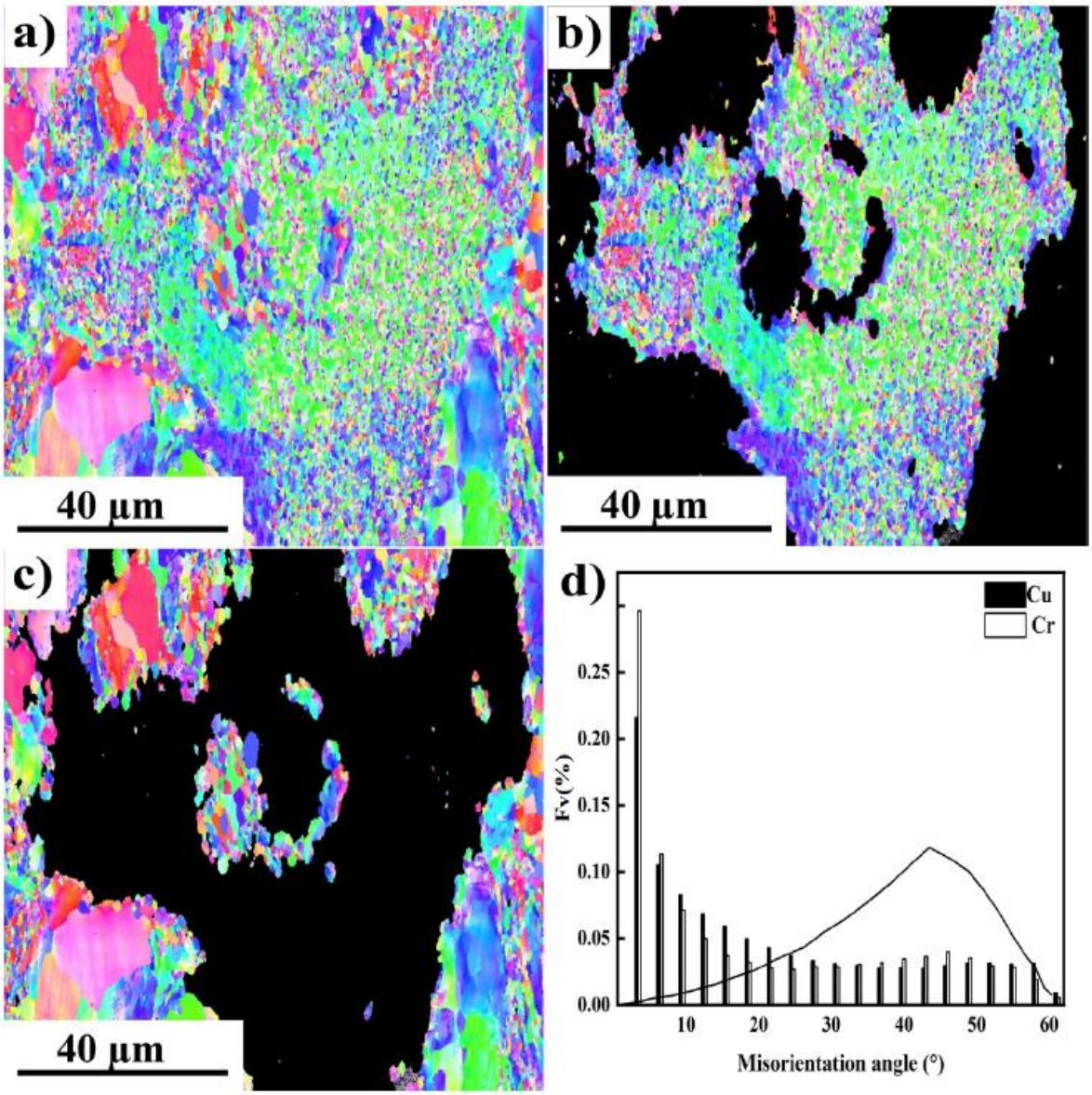

Figure 2: Characteristics of the Cu43%Cr alloy in the as-received state, a) SEM-EBSD patterns in the CD-IPF mode in Cu43%Cr alloy, b) in Cu phase and c) in Cr phase, d) misorientation angle histograms.

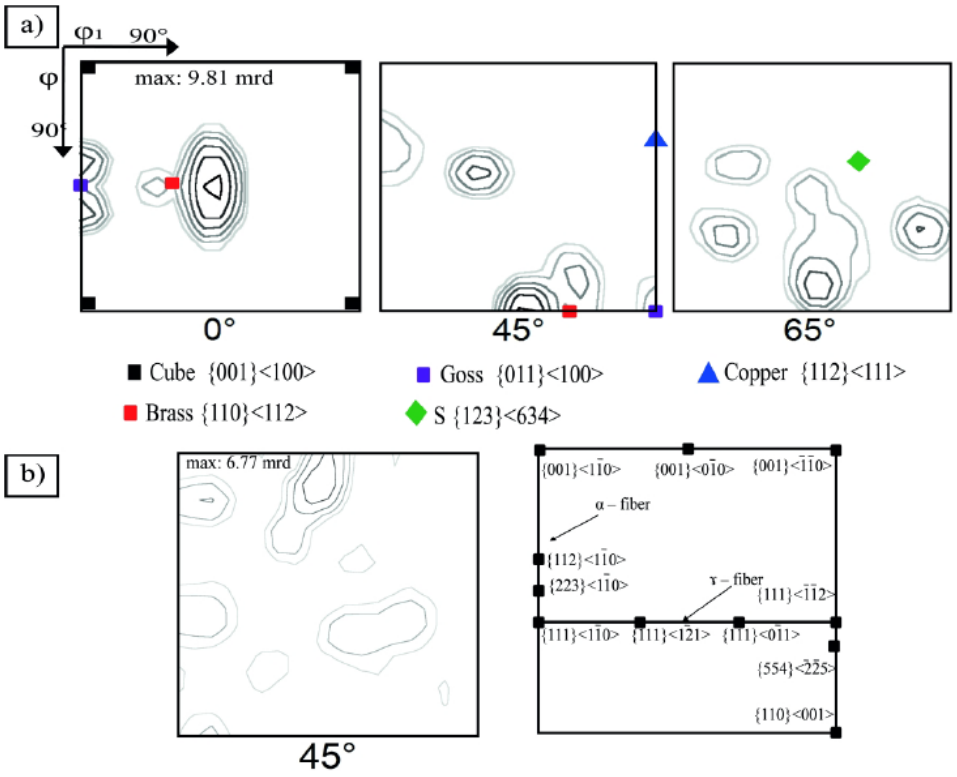

Figure 3 : ODF sections of the Cu43%Cr alloy in the as-received state, a) at φ_2 =0, 45 and 65° for the Cu phase, b) at φ_2 =45° for Cr phase.

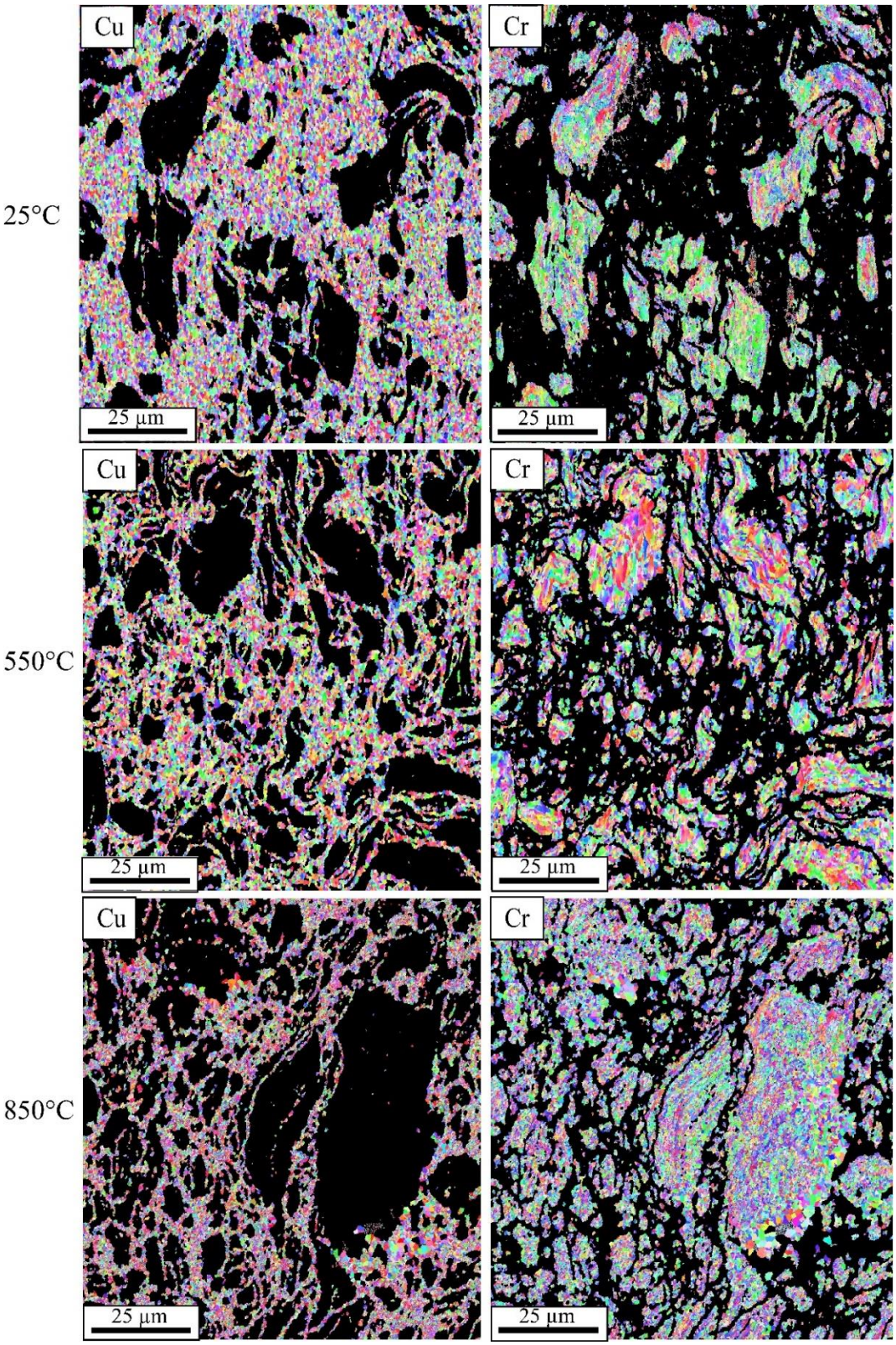

Figure 4: Orientation imaging micrographs (CD-IPF mode) of the Cu (left) and Cr (right) in the Cu43%Cr alloy after 5 turns HPT (25°C) and annealing at 550°C and 850°C.

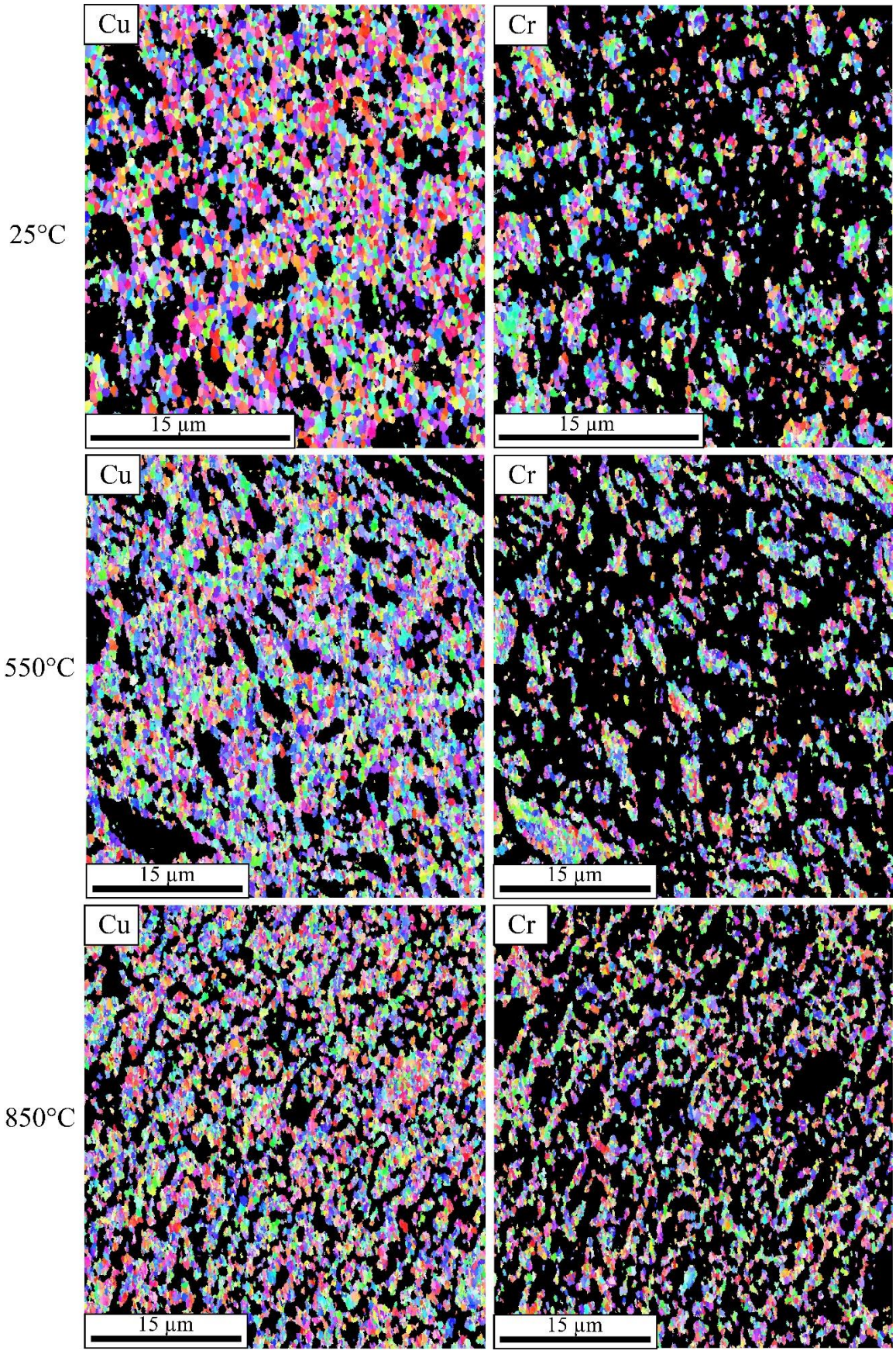

Figure 5: Orientation imaging micrographs (CD-IPF mode) of the Cu (left) and Cr (right) in the Cu43%Cr alloy after 20 turns HPT (25°C) and annealing at 550°C and 850°C.

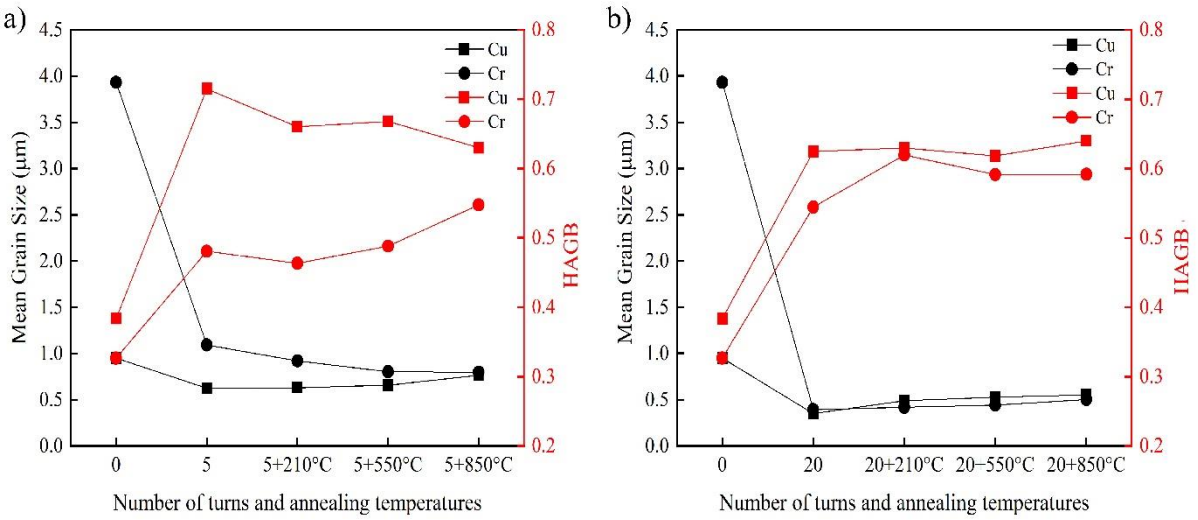

Figure 6: Evolution of the mean grain size and high-angle grain boundary fraction (HAGB) of the Cu43%Cr alloy after HPT processing up to a) N= 5 and b) N=20 HPT turns and annealing

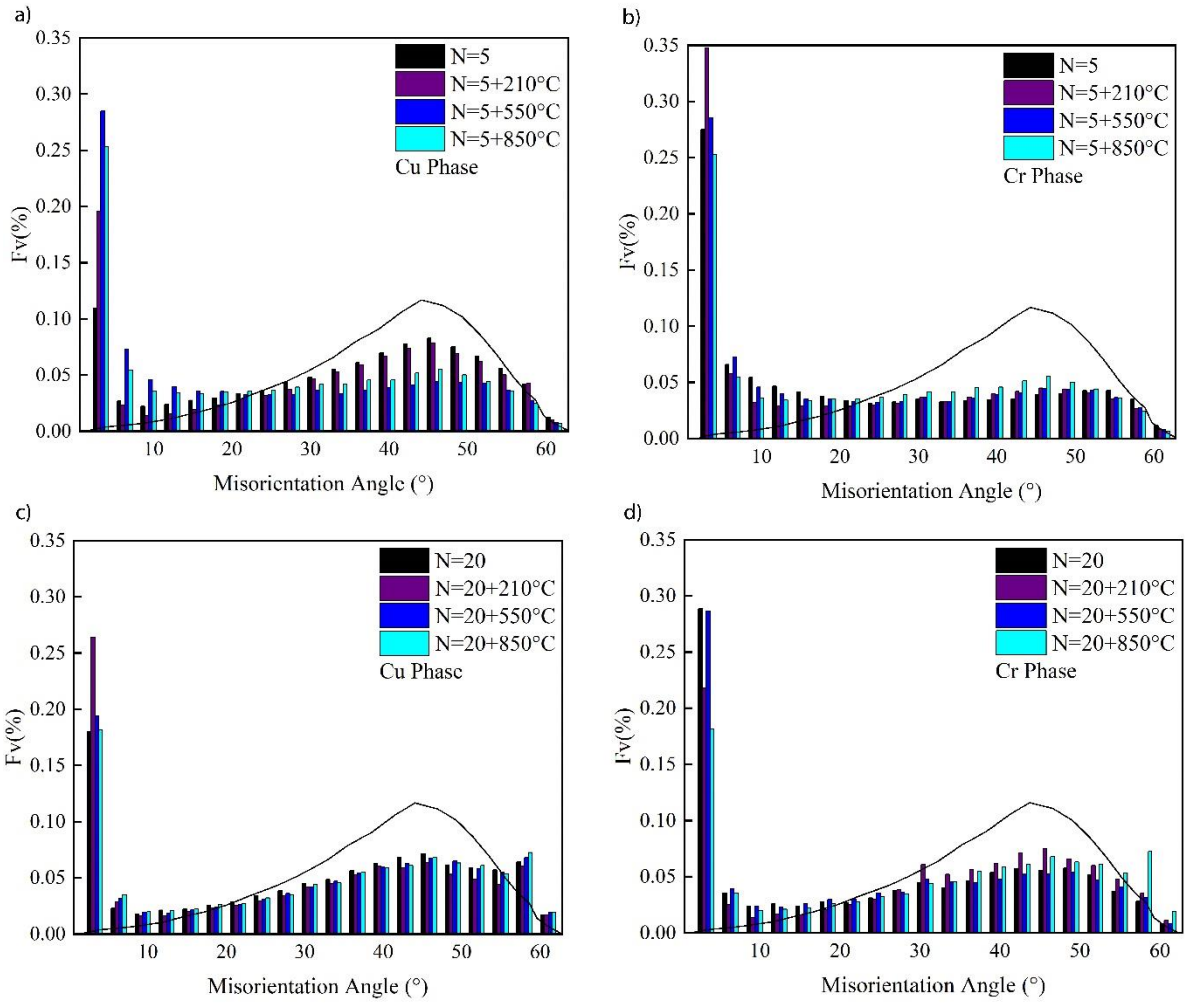

Figure 7: Histograms of the grain boundary misorientation angles after HPT processing and annealing of the Cu43%Cr alloy, a) Cu (N=5), b) Cr (N=5), c) Cu (N=20) and d) Cr (N=20) phases.

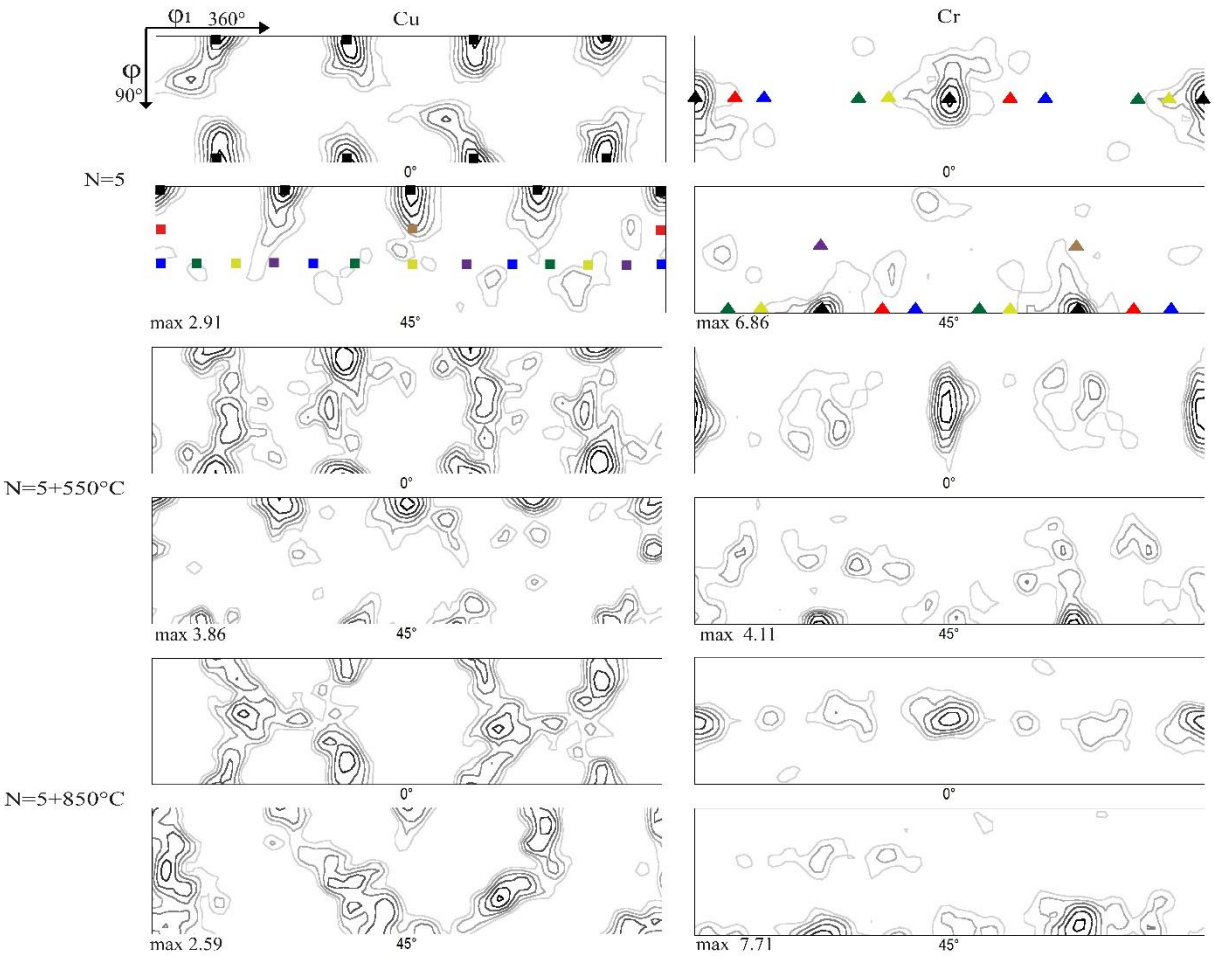

Figure 8: ODF section at φ_2 = 0 and 45° of the Cu43%Cr alloy after 5 turns HPT and annealing.

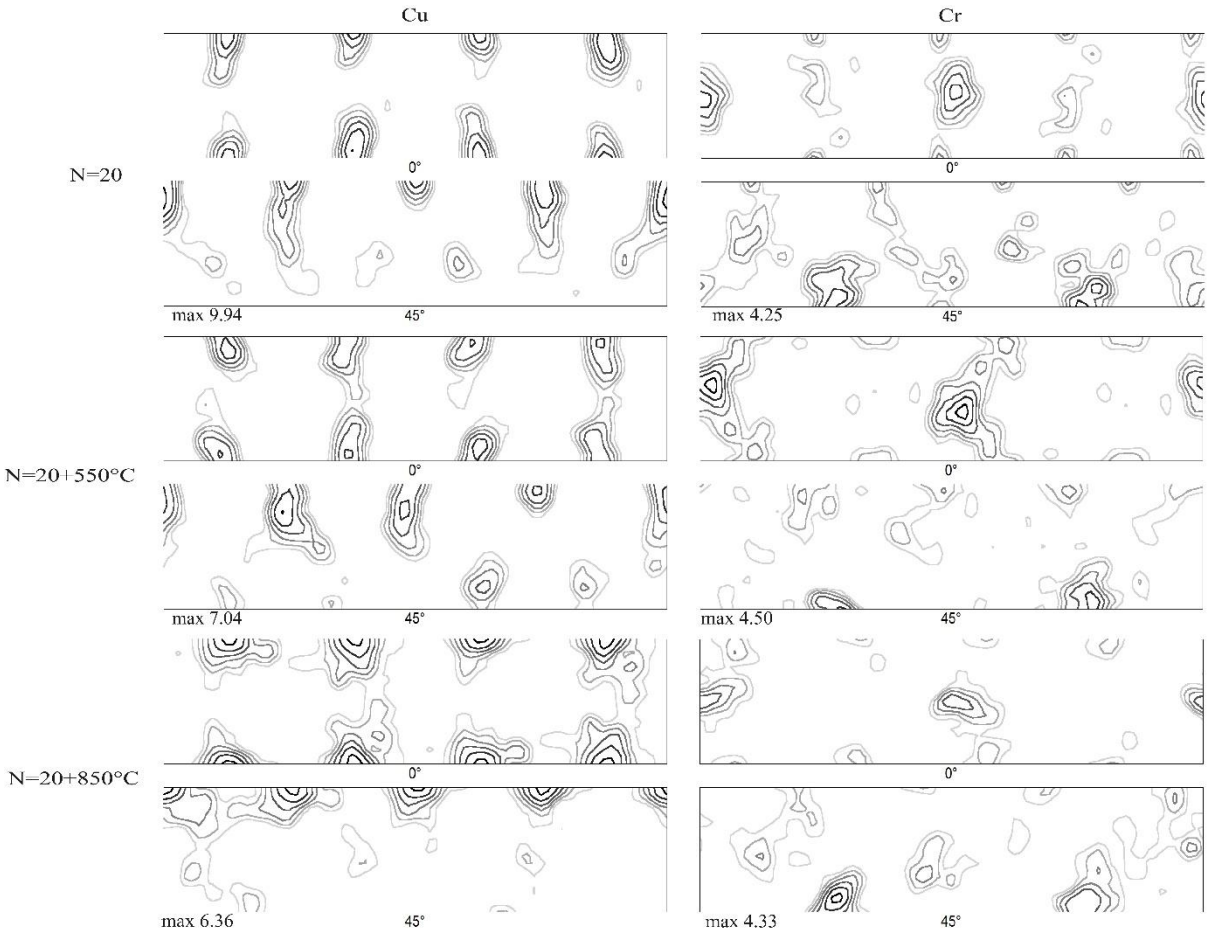

Figure 9: ODF section at φ_2 = 0 and 45° of the Cu43%Cr alloy after 20 turns HPT and annealing.

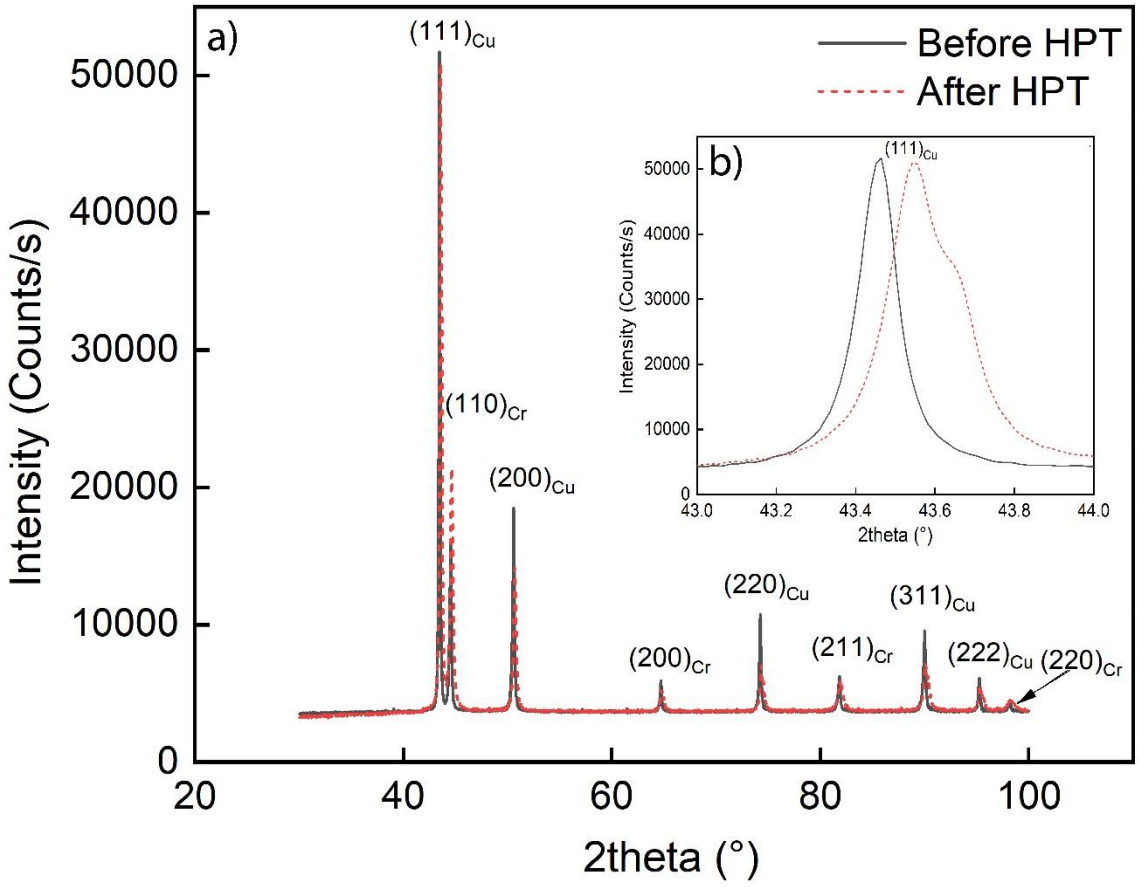

Figure 10: (a) XRD analysis of the Cu43%Cr alloy before and after HPT processing (20 turns) and b) zoom of an area near the $(111)_{Cu}$.

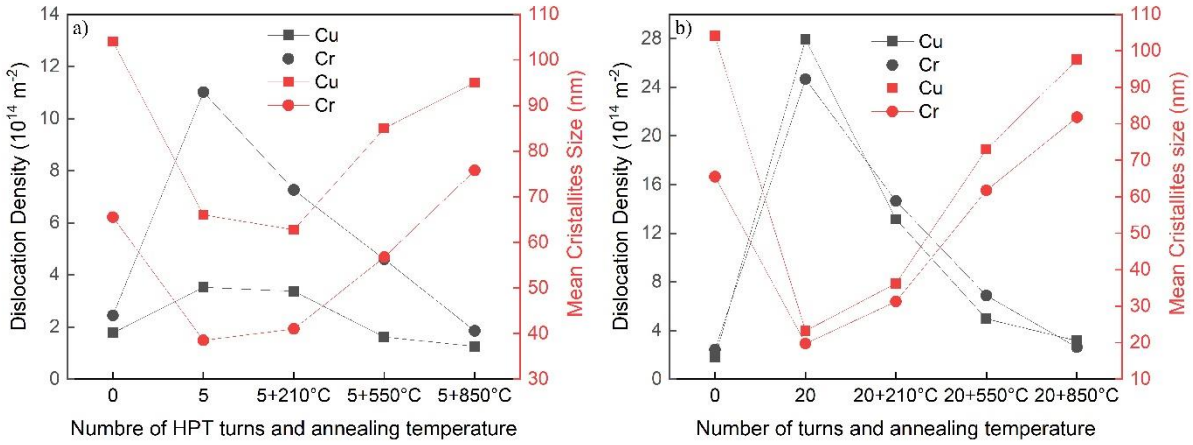

Figure 11: Evolution of the dislocation density and the mean crystallite size of the Cu43%Cr alloy after HPT processing and annealing.

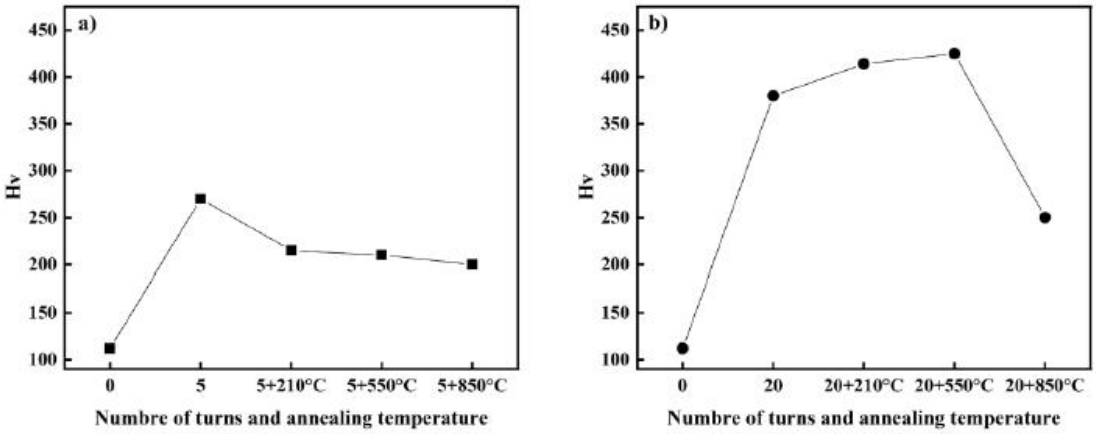

Figure 12: Evolution of the global microhardness of the Cu43%Cr alloy after HPT processing and annealing.

Table 1: Position of ideal shear texture components for FCC metals and alloys projected in SD-RD plane.

Notation	Miller indice {hkl}<uvw>
A	$\{1\bar{1}1\}\langle 110\rangle$
$\bar{A}$	$\{\bar{1}1\bar{1}\}\langle\bar{1}\bar{1}0\rangle$
A_1^*	$\{11\bar{1}\}\langle 112\rangle$
A_2^*	$\{11\bar{1}\}\langle 2\bar{1}1\rangle$
B	$\{1\bar{1}2\}\langle 110\rangle$
$\bar{B}$	$\{\bar{1}1\bar{2}\}\langle\bar{1}\bar{1}0\rangle$
C	$\{001\}\langle 110\rangle$

Table 2: Position of ideal shear texture components for BCC metals and alloys projected in SD-RD plane.

Notation	Miller indice {hkl}<uvw>
D_1	$\{\bar{1}\bar{1}2\}<111>$
D_2	$\{11\bar{2}\}<111>$
J	$\{\bar{1}\bar{1}0\}<112>$
$\bar{J}$	$\{0\bar{1}1\}<\bar{2}11>$
E	$\{110\}<1\bar{1}1>$
$\bar{E}$	$\{1\bar{1}0\}<\bar{1}1\bar{1}>$
F	$\{110\}<001>$

Table 3: Lattice parameter, crystallite size and dislocations density of Cu and Cr phases in Cu43%Cr alloy after HPT processing and annealing for 1 hour at 210, 550 and 850°C.

Phase	Cu			Cr		
Expérimental Conditions	a (nm)	<D> (nm)	ρ ($10^{14}m^{-2}$)	a (nm)	<D>(nm)	ρ ($10^{14}m^{-2}$)
N=5	0.3617	66	3.522	0.2890	38.5	11.013
N=5+210°C	0.3617	62.75	3.373	0.2888	41	7.261
N=5+550°C	0.3617	85	1.614	0.2883	56.75	4.598
N=5+850°C	0.3618	95.25	1.257	0.2886	75.75	1.858
N=20	0.3617	23.25	27.934	0.2890	19.75	24.677
N=20+210°C	0.3617	36.25	13.145	0.2887	31.25	14.643
N=20+550°C	0.3617	73	4.950	0.2886	61.75	6.877
N=20+850°C	0.3618	97.5	3.156	0.2887	81.75	2.612